Communication

Live-cell STED microscopy with genetically encoded biosensor

Natalie M Mishina, Alexander S Mishin, Yury Belyaev, Ekaterina A Bogdanova, Sergey Lukyanov, Carsten Schultz, and Vsevolod V. Belousov

Nano Lett., **Just Accepted Manuscript** • Publication Date (Web): 14 Apr 2015

Live-cell STED microscopy with genetically encoded biosensor

Natalia M. Mishina[1,2], Alexander S. Mishin[1,2], Yury Belyaev[3], Ekaterina A. Bogdanova[1], Sergey Lukyanov[1,2], Carsten Schultz[3], Vsevolod V Belousov[1,2]*

[1]Shemyakin-Ovchinnikov Institute of Bioorganic Chemistry, Moscow, Russia

[2]Nizhny Novgorod State Medical Academy, Nizhny Novgorod, Russia

[3]EMBL Heidelberg, Heidelberg, Germany

ABSTRACT Of the various super-resolution techniques, stimulated emission depletion (STED) microscopy achieves the best temporal resolution at high spatial resolution enabling live-cell imaging beyond the diffraction limit. However, STED and most other super-resolution imaging methods utilize a particular type of information extractable from the raw data, namely the positions of fluorophores. To expand on the use of super-resolution techniques, we here report live-cell STED microscopy of a dynamic biosensor. Using the fluorescent H_2O_2 sensor HyPer2 for subdiffraction imaging, we were able not only to image filaments with superior resolution by localizing emission, but also to trace H_2O_2 produced within living cell by monitoring brightness of the probe. STED microscopy of HyPer2 demonstrates potential utility of FP-based biosensors for super-resolution experiments *in situ* and *in vivo*.

KEYWORDS Microscopy, biosensor, super-resolution imaging, hydrogen peroxide, STED, HyPer

Fluorescent imaging is one of the most powerful techniques in modern biology. In past decades, several revolutions radically changed this field. Among them, appearance of fluorescent biosensors allowed dynamic tracking of second messengers, metabolites and enzymatic activities in living systems[1]. Recently, development of subdiffraction imaging dramatically lowered the resolution limit of fluorescence microscopy[2–5]. Subdiffraction microscopy produces images based on positions of individual fluorophores, either small molecule dyes[6–8] or fluorescent proteins[9]. The fluorophores are most often linked to subcellular structures such as cytoskeleton filaments or other relatively stable multimolecular intracellular structures[10,11]. However, super-resolution imaging utilizes predominantly the position of individual fluorophores as the sole information extractable from the raw data. The question arises if it is possible to extract information from dynamic processes by subdiffraction imaging, potentially along with subcellular structures resolution. A first step towards resolving these issues would be using a biosensor as a fluorophore for subdiffraction imaging. Whereas single molecule localization imaging modalities, such as PALM/STORM[2,12] are rather slow and require analysis of information from single-molecules, stimulated emission depletion (STED) microscopy[4] provides ensemble spectral data and seems to be a suitable method for biosensor imaging.

HyPer2, an improved version of H_2O_2 biosensor HyPer[13], consists of a mutated H_2O_2-sensitive bacterial protein domain (OxyR-RD) and circularly permuted yellow fluorescent protein (cpYFP)[14]. Targeting of HyPer to subcellular compartments already provided insight to the diffusion-limited nature of hydrogen peroxide signaling[15].

For STED, a number of YFP-like proteins have been used so far[9,16], and since HyPer2 is based on a circularly permuted YFP variant, we decided to apply this sensor in STED. Fusing HyPer2 with cytoskeleton structures would allow not only subdiffraction imaging of filaments by localizing emission, but also imaging of H_2O_2 produced within the cell by monitoring of HyPer2 brightness.

Fluorophores for STED need to be particularly photostable because of the high energy of light required for emission stimulation/depletion[9]. We therefore analyzed the photostability of HyPer2 and its variants in comparison to other YFPs. We found that HyPer2 exhibits surprisingly high photostability compared to related fluorescent proteins of a similar spectrum (Figure 1).

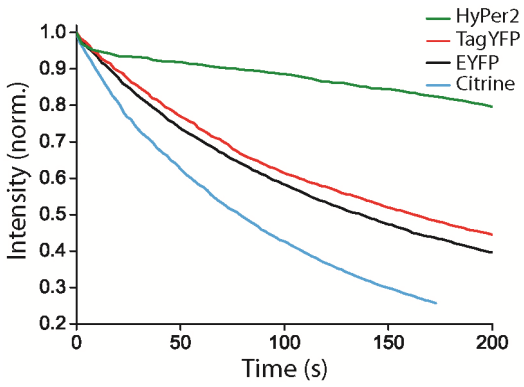

Figure 1. Photobleaching curves for HyPer2 (green), TagYFP (red), EYFP (black), and Citrine (blue), expressed in HeLa-Kyoto cells during live-cell widefield microscopy (100W arc-lamp, 40x oil objective, FITC filter set).

In order to investigate HyPer2 by STED, we fused it with vimentin and imaged transfected HeLa-Kyoto cells using confocal and STED microscopy. We observed an up to 3-fold enhancement in resolution in STED images compared to the confocal mode (Figure 2A,B, also compare to Vimentin-Citrine - Figure S1, Supporting Information). Therefore, YFP-based biosensors such as HyPer2 appear to be suitable fluorophores for subdefraction imaging. We

then tested HyPer2 performance as a sensor in the same cells. Under conventional confocal imaging conditions the fluorescence intensity of HyPer2 fused to vimentin changed two- to three-fold upon saturation with H_2O_2 (Figure S2, Supporting Information). In STED mode, a three- to five-fold elevation of HyPer2 fluorescence intensity was observed upon addition of exogenous H_2O_2 to the cells. (Figure 2C,D and Video S1, Supporting Information). Thus, despite the high intensity of the excitation and depletion beams, HyPer2 retained its sensitivity to H_2O_2 and was able to change the brightness of cpYFP fluorophore in response to the oxidant. Moreover, we were able to detect a dose-dependent increase in HyPer2 brightness in response to H_2O_2 in STED mode whereas the Vimentin-Citrine fusion showed just bleaching under the same conditions (Figure S3, Supporting Information).The minimal concentration of external H_2O_2 that induced detectable response of HyPer2 was 800 nM. Given the existence of a 200-500 fold gradient of H_2O_2 across the plasma membrane[17,18], this concentration corresponds to as low as 2-4 nM H_2O_2 in the cytoplasm.100 μM H_2O_2 (~200 nM intracellular) almost completely saturated the sensor (Figure S3, Supporting Information).

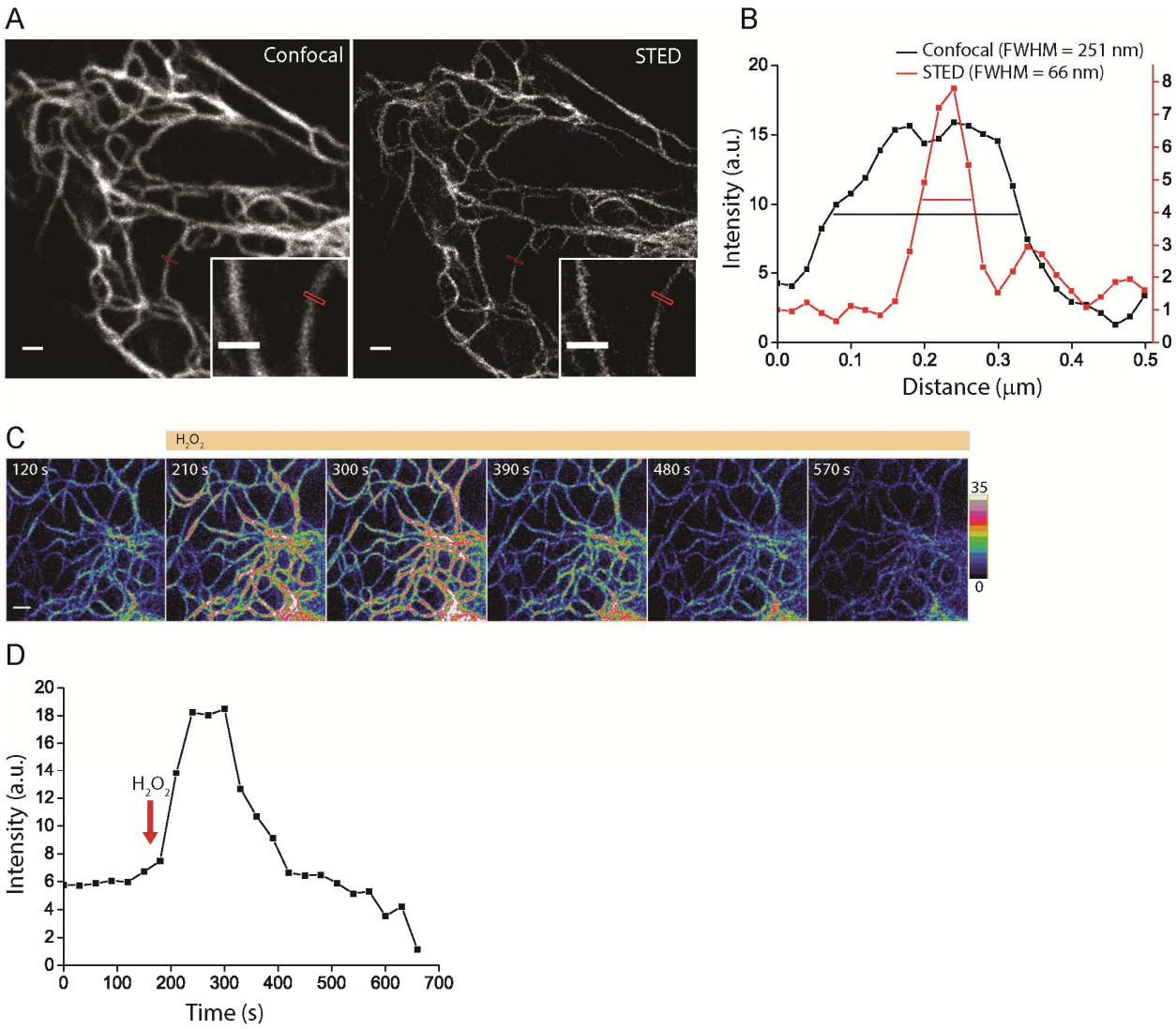

Figure 2. Live-cell imaging of H_2O_2 by HyPer2. (A) Confocal and STED images of live HeLa-Kyoto cell expressing Vimentin-HyPer2. The box denotes the region of interest. Scale bar: 1 μm. (B) Line profiles correspond to the averaged fluorescence intensity within the region of interest from panel (A) plotted as a function of distance. (C) STED images of live Vimentin-HyPer2-expressing HeLa-Kyoto cell at indicated time points. H_2O_2 (200 μM) was added between the 1st and 2nd frame shown (see Video S1, Supporting Information). Scale bar: 1 μm. (D) Timing of the fluorescence intensity change in the cell shown in panel (C). This experiment is representative of 3 repeats.

Cells use hydrogen peroxide for signaling[19]. Mostly, H_2O_2 reacts with low pKa thiol residues of proteins causing reversible oxidation and disulfide bonds formation[20].One of the examples of such redox signaling is the H_2O_2-induced oxidation of catalytic sites of protein tyrosine phosphatases in response to receptor tyrosine kinases (RTK) activation by growth factors[21–24]. Such transient inactivation of PTPs enables downstream targets phosphorylation by RTKs. H_2O_2 is a rather stable and well diffusible molecule that travels several millimeters in water. However, the cytoplasm contains a high concentration of peroxiredoxins (Prxs), highly abundant antioxidant enzymes that have an extremely high reaction rate with H_2O_2[25]. Theoretical calculation predicted that even redox sensitive low pKa protein thiols would be unable to compete with Prxs for H_2O_2[26]. However, experimental data clearly show many examples of oxidative regulation by thiols. To fit theoretical and experimental data, a model called "floodgate" was suggested. One of the features of Prx is that it can be overoxidized and hence inactivated by H_2O_2[27]. The floodgate model suggests that H_2O_2 concentrations near the site of its generation are sufficiently high to inactivate Prx transiently, thus enabling oxidation of other thiols in the close proximity of oxidized Prx. Each H_2O_2 generation site is surrounded by a small "cloud" of H_2O_2 that acts locally, near the site of its generation. In support of the floodgate model, we demonstrated earlier that placing the HyPer sensors close to the site of H_2O_2 production leads to much more intensive fluorescence changes compared to a non-localized diffusible version of the probe when responding to growth factor stimulation of the cells[15]. Using conventional fluorescence microscopy, we were able to show that, for example, two H_2O_2 generating endosomes separated by a distance of 1-2 μm show a different HyPer signal. This means that H_2O_2 is unable to cross even this small distance[15]. But what is the real size of this H_2O_2 "cloud"? Would we be able to answer this question by using STED microscopy?

In order to address these questions we fused HyPer2 with the microtubule end binding protein EB3 and expressed this fusion in NIH 3T3 fibroblasts. We were able to localize microtubules in living cells (Figure 3A, B). Fibroblasts express PDGFR, a tyrosine kinase receptor for platelet derived growth factor (PDGF). Addition of 10 ng/ml PDGF to cells induced a sustained increase in cellular H_2O_2 levels over time reflected by profound increases of EB3-HyPer2 brightness. Addition of external H_2O_2 induced a further increase in brightness, finally saturating the probe (Figure 3B,C and Video S2, Supporting Information). Negative control with addition of serum-free medium without PDGF to the cells demonstrated only photobleaching of EB3-HyPer2 (Figure S4, Supporting Information).

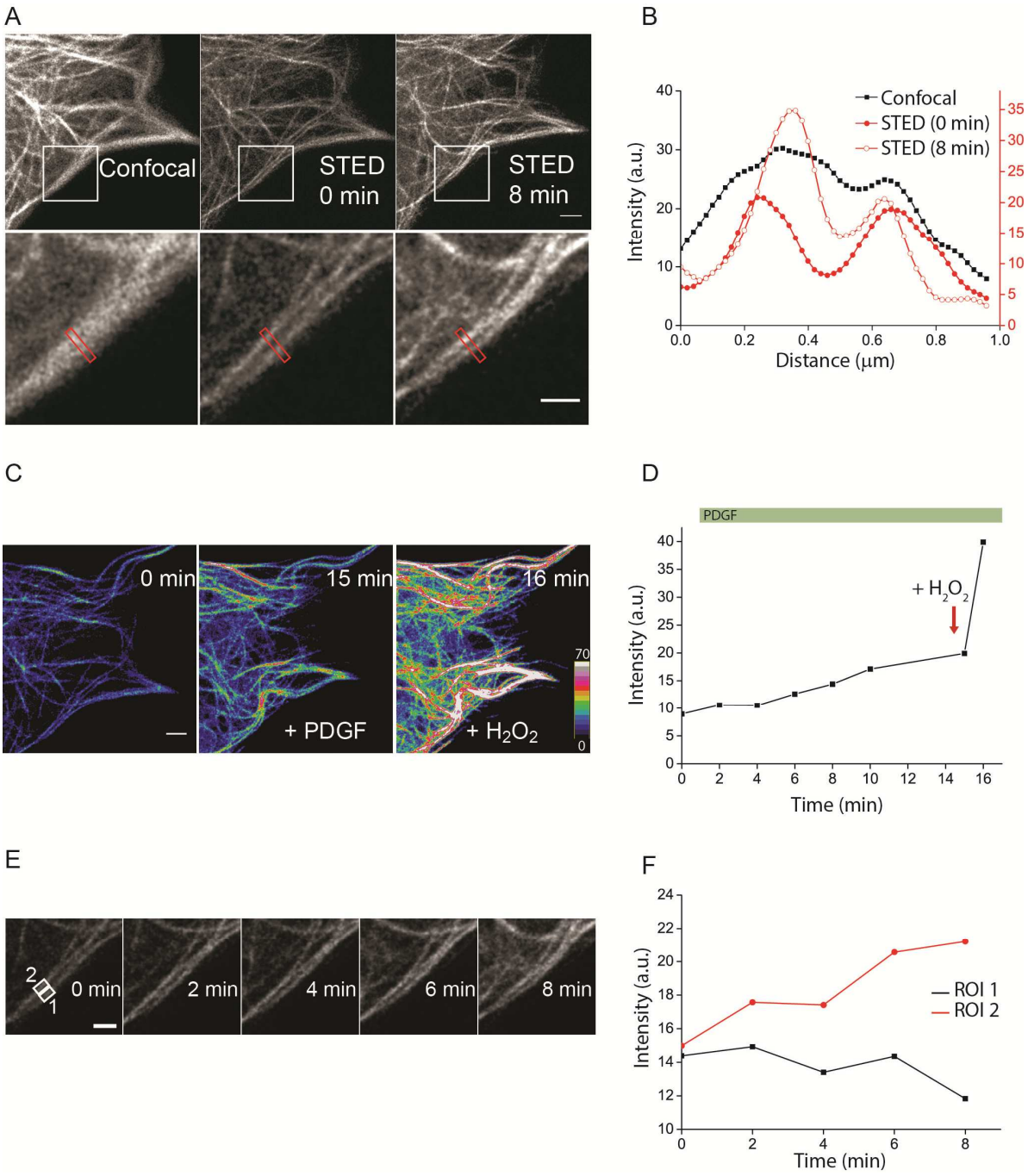

Figure 3. Imaging of EB3-HyPer2 in live NIH 3T3 cells. (A) Confocal (left column) and STED (middle and right column) images of microtubules labeled with EB3-HyPer2. STED images show cell after stimulation with 10 ng/ml PDGF: middle column (0 min) corresponds to the moment of PDGF addition, right column to 8 min after PDGF addition. Lower row corresponds to inserts in the upper row. Red box denotes the region of interest (ROI). Scale bar: 2 μm (upper

row), 1 μm (lower row). (B) Line profiles through the two adjacent microtubules (along the marked red box in lower row of panel A) demonstrate nearly equal intensity peaks at the moment of stimulation with PDGF (STED 0 min, red line with filled circles) and subsequent change in intensity peaks 8 min after stimulation (STED 8 min, red line with empty circles). Note that in confocal mode these two microtubules are not resolved (black line with squares). (C) STED images of EB3-Hyper2 fluorescence intensity change in NIH 3T3 cell at indicated time points after stimulation with 10 ng/ml PDGF and subsequent addition of 200 μM H_2O_2 (see Video S2, Supporting Information). H_2O_2 was added between the 2nd and 3rd frame. Scale bar: 2 μm. (D) Timing of fluorescence intensity change in cell shown on panel (C).(E) STED images of EB3-Hyper2 fluorescence intensity change in NIH 3T3 cell at indicated time points after stimulation with 10 ng/ml PDGF. Scale bar: 1 μm. (F) Timing of fluorescence intensity change in ROIs (from panel C) demonstrates the difference in HyPer2-labelled adjacent microtubules response to internal H_2O_2 production.

Analysis of the STED imaging series revealed the presence of pairs of microtubules that, despite the close proximity to each other, demonstrated different dynamics of changes in HyPer2 brightness (Figure 3E,F). Note that these filaments were so close to each other that conventional confocal microscopy was unable to resolve them (Figure 3A,B). This difference in HyPer2 dynamics between neighboring filaments indicates that microdomains of H_2O_2 in the cytoplasm can be as small as 100-200 nm in linear size. Due to the increased motility of stimulated cells it was challenging to localize pairs of filaments that remained in the close proximity to each other throughout the entire time series. However, we were able to localize a number of such pairs that

demonstrated unequal changes in HyPer2 signals between two sequential time frames (Figure S5, Supporting Information).

Together, our experiments show that the size of H_2O_2 microdomains can be estimated with much better precision using super-resolution microscopy than using widefield or confocal imaging. This provides striking evidence that cells control the location of the oxidant used for cell signaling with high spatial precision thus ensuring that mislocalized H_2O_2 would not cause off-target oxidation known as "oxidative stress". More generally, our experiments indicate that fluorophore brightness is suitable as a readout in live cell STED imaging providing additional information about dynamic processes in the cell along with information on the filament structure.

What are the limitations and perspectives of subdiffraction imaging with biosensors? The first limitation is the relatively low brightness of HyPer2 and similar biosensors[18]. Development of brighter versions would help to achieve lower irradiation intensities that would be beneficial for live cell imaging. Second, despite the fairly high photostability of HyPer2 in conventional microscopy (Figure 1), in STED photobleaching rates of Hyper2 and Citrine were similar (Figure 4). Therefore, photostability should be further improved.

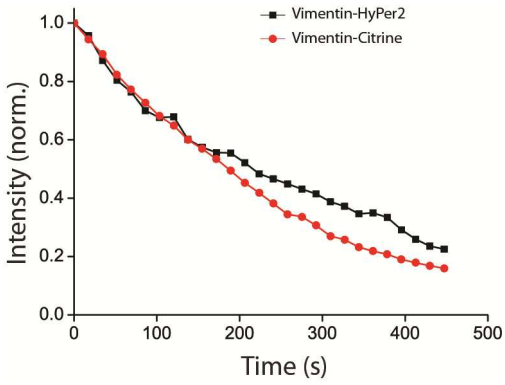

Figure 4. Normalized STED microscopy photobleaching curves of HyPer2 and Citrine fused to vimentin and imaged in live HeLa-Kyoto cells.

Third, low acquisition speed limits the potential use of subdiffraction imaging for fast processes such as neuronal Ca^{2+} dynamics. This also dictates a need for tethering the probes within the cell using fusions with low-mobility proteins. Otherwise, fast diffusion of the non-fused indicator would lead to the loss of spatial signal heterogeneity. In perspective, as the speed of subdiffraction imaging increases, it would be extremely important to investigate dynamics of second messengers using STED- or PALM/STORM-like approaches. We would be able to see subdiffraction images of H_2O_2 or Ca^{2+} distribution within the living cells just like we see now structures of supramolecular complexes. Our data on HyPer2 imaging in STED mode indicate that these exciting experiments will be possible in the closest future.

FIGURES

Figure 1.

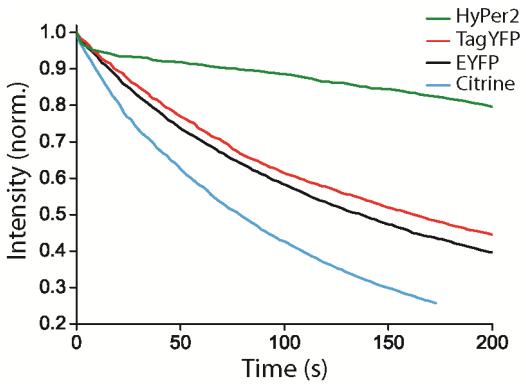

Figure 1. Photobleaching curves for HyPer2 (green), TagYFP (red), EYFP (black), and Citrine (blue), expressed in HeLa-Kyoto cells during live-cell widefield microscopy (100W arc-lamp, 40x oil objective, FITC filter set).

Figure 2.

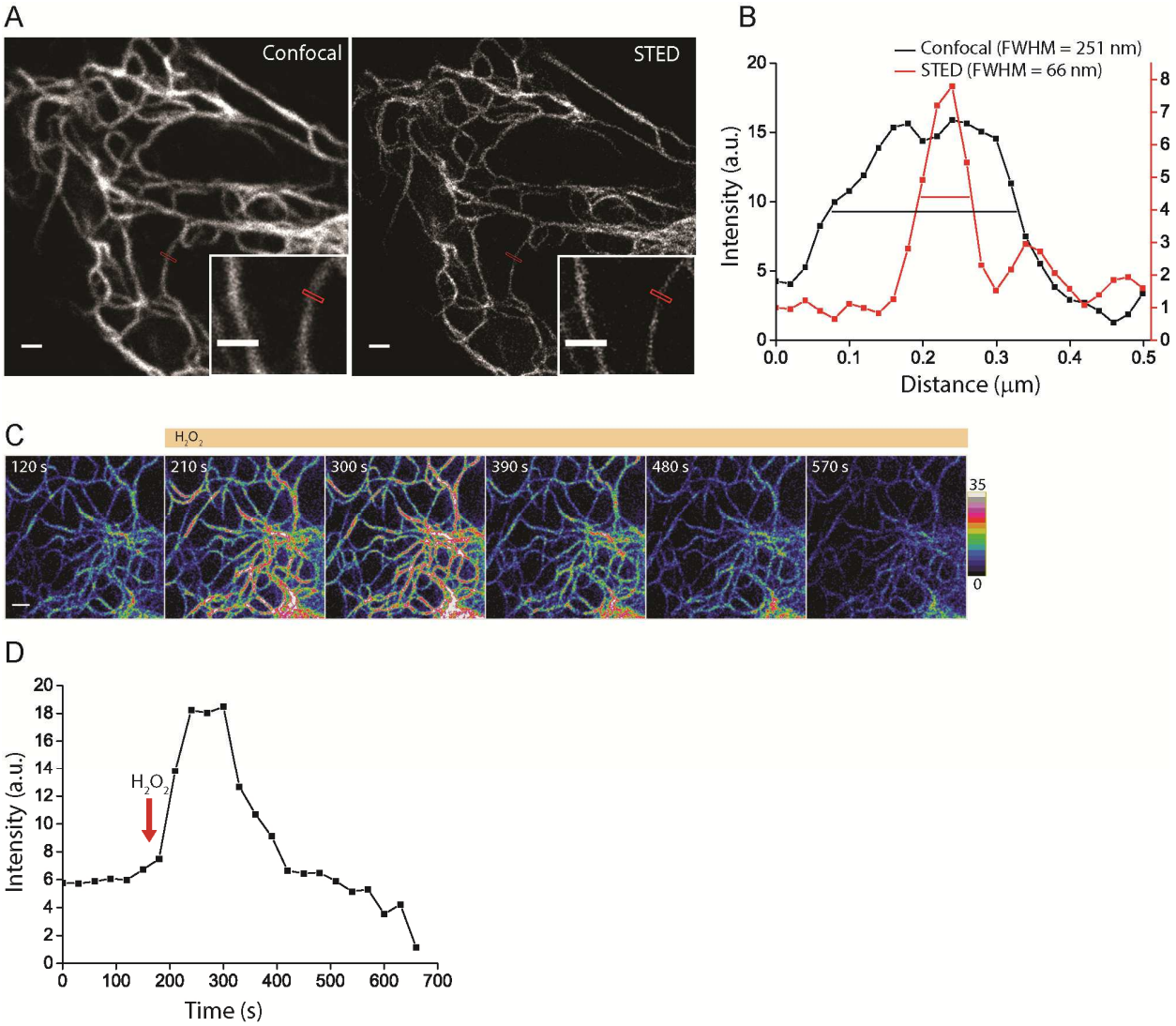

Figure 2. Live-cell imaging of H_2O_2 by HyPer2. (A) Confocal and STED images of live HeLa-Kyoto cell expressing Vimentin-HyPer2. The box denotes the region of interest. Scale bar: 1 μm. (B) Line profiles correspond to the averaged fluorescence intensity within the region of interest from panel (A) plotted as a function of distance. (C) STED images of live Vimentin-HyPer2-expressing HeLa-Kyoto cell at indicated time points. H_2O_2 (200 μM) was added between the 1st and 2nd frame shown (see Video S1, Supporting Information). Scale bar: 1 μm. (D) Timing of the fluorescence intensity change in the cell shown in panel (C). This experiment is representative of 3 repeats.

Figure 3.

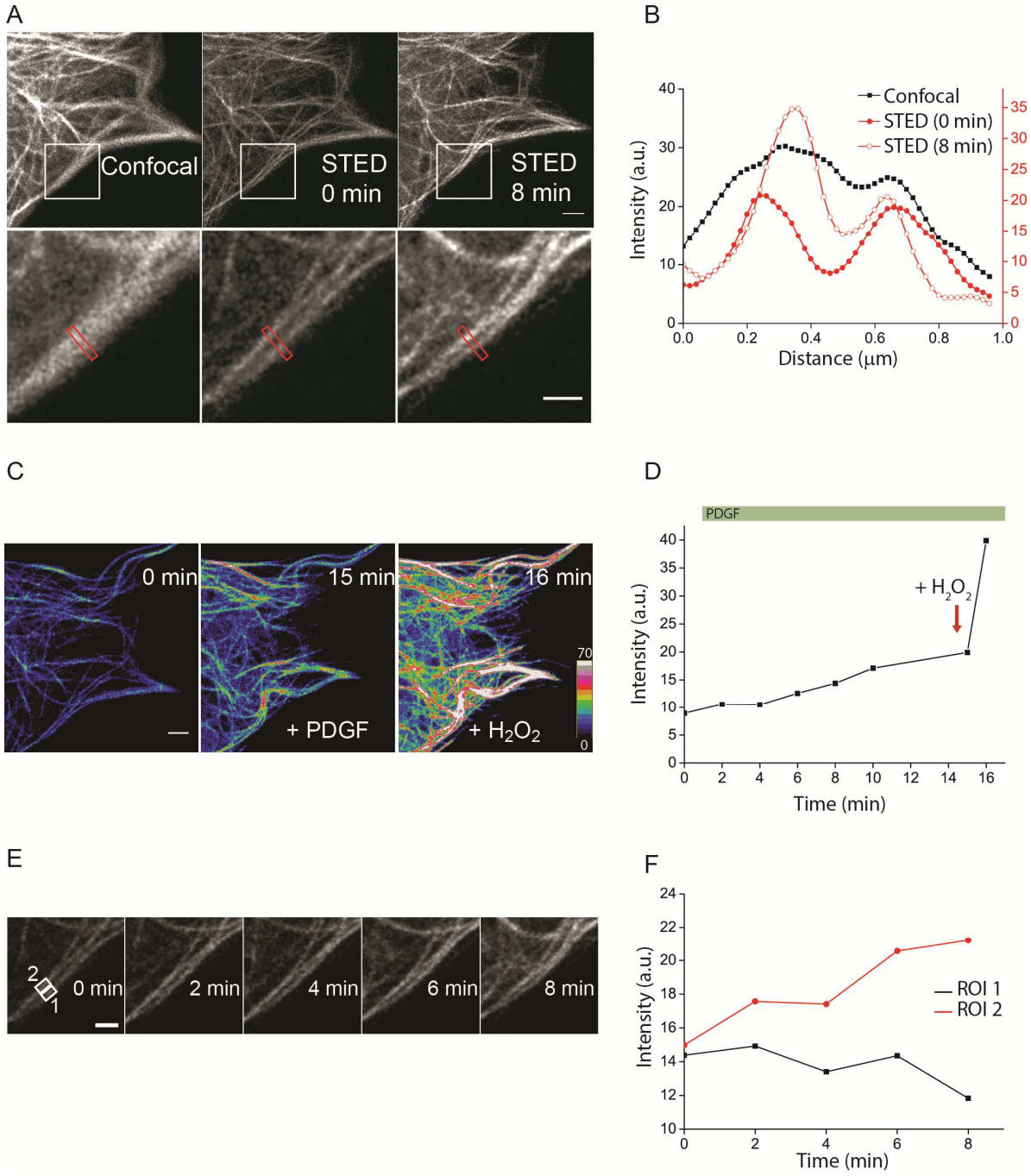

Figure 3. Imaging of EB3-HyPer2 in live NIH 3T3 cells. (A) Confocal (left column) and STED (middle and right column) images of microtubules labeled with EB3-HyPer2. STED images show cell after stimulation with 10 ng/ml PDGF: middle column (0 min) corresponds to the moment of PDGF addition, right column to 8 min after PDGF addition. Lower row corresponds

to inserts in the upper row. Red box denotes the region of interest (ROI). Scale bar: 2 μm (upper row), 1 μm (lower row). (B) Line profiles through the two adjacent microtubules (along the marked red box in lower row of panel A) demonstrate nearly equal intensity peaks at the moment of stimulation with PDGF (STED 0 min, red line with filled circles) and subsequent change in intensity peaks 8 min after stimulation (STED 8 min, red line with empty circles). Note that in confocal mode these two microtubules are not resolved (black line with squares). (C) STED images of EB3-Hyper2 fluorescence intensity change in NIH 3T3 cell at indicated time points after stimulation with 10 ng/ml PDGF and subsequent addition of 200 μM H_2O_2 (see Video S2, Supporting Information). H_2O_2 was added between the 2^{nd} and 3^{rd} frame. Scale bar: 2 μm. (D) Timing of fluorescence intensity change in cell shown on panel (C).(E) STED images of EB3-Hyper2 fluorescence intensity change in NIH 3T3 cell at indicated time points after stimulation with 10 ng/ml PDGF. Scale bar: 1 μm. (F) Timing of fluorescence intensity change in ROIs (from panel C) demonstrates the difference in HyPer2-labelled adjacent microtubules response to internal H_2O_2 production.

Figure 4.

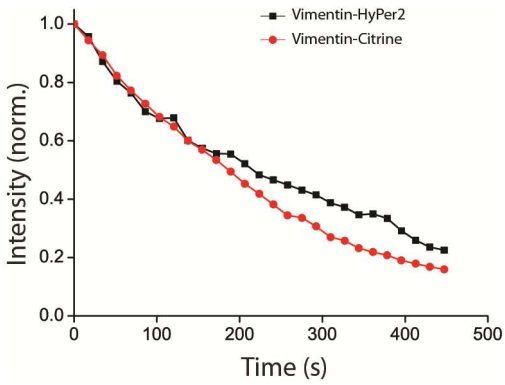

Figure 4. Normalized STED microscopy photobleaching curves of HyPer2 and Citrine fused to vimentin and imaged in live HeLa-Kyoto cells.

ASSOCIATED CONTENT

Supporting Information. A Materials and Methods section, additional figures and video. This material is available free of charge via the Internet at http://pubs.acs.org.

AUTHOR INFORMATION

Corresponding Author

*Vsevolod V. Belousov; phone +7-499-7248466, fax +7-495-3307056, e-mail: vsevolod.belousov@gmail.com

Notes

The authors declare no competing financial interest.

ACKNOWLEDGMENT

We thank the Advanced Light Microscopy Facility (ALMF) at the European Molecular Biology Laboratory (EMBL) and Leica Microsystems for support. This work was supported by the Russian foundation for basic research (13-04-40333-H to V.V.B), EMBL-RFBR grant 15-54-74003 to C.S. and V.V.B, Molecular and Cell Biology program of Russian Academy of Sciences (V.V.B).

REFERENCES

(1) Newman, R. H.; Fosbrink, M. D.; Zhang, J.. *Chem. Rev.* **2011**, *111*, 3614–3666.

(2) Betzig, E.; Patterson, G. H.; Sougrat, R.; Lindwasser, O. W.; Olenych, S.; Bonifacino, J. S.; Davidson, M. W.; Lippincott-Schwartz, J.; Hess, H. F. *Science* **2006**, *313*, 1642–1645.

(3) Hess, S. T.; Girirajan, T. P. K.; Mason, M. D. *Biophys. J.* **2006**, *91*, 4258–4272.

(4) Hell, S. W.; Wichmann, J. *Opt. Lett.* **1994**, *19*, 780–782.

(5) Bates, M.; Huang, B.; Dempsey, G. T.; Zhuang, X. *Science* **2007**, *317*, 1749–1753.

(6) Westphal, V.; Rizzoli, S. O.; Lauterbach, M. A.; Kamin, D.; Jahn, R.; Hell, S. W. *Science* **2008**, *320*, 246–249.

(7) Kasper, R.; Harke, B.; Forthmann, C.; Tinnefeld, P.; Hell, S. W.; Sauer, M. *Small* **2010**, *6*, 1379–1384.

(8) Bates, M.; Jones, S. a; Zhuang, X. *Cold Spring Harb. Protoc.* **2013**, *2013*, 498–520.

(9) Nienhaus, K.; Nienhaus, G. U. *Chem. Soc. Rev.* **2014**, *43*, 1088–1106.

(10) Sengupta, P.; Van Engelenburg, S.; Lippincott-Schwartz, J. *Dev. Cell* **2012**, *23*, 1092–1102.

(11) Eggeling, C.; Willig, K. I.; Barrantes, F. J. *J. Neurochem.* **2013**, *126*, 203–212.

(12) Rust, M. J.; Bates, M.; Zhuang, X. *Nat. Methods* **2006**, *3*, 793–795.

(13) Belousov, V. V; Fradkov, A. F.; Lukyanov, K. A.; Staroverov, D. B.; Shakhbazov, K. S.; Terskikh, A. V; Lukyanov, S. *Nat. Methods* **2006**, *3*, 281–286.

(14) Markvicheva, K. N.; Bilan, D. S.; Mishina, N. M.; Gorokhovatsky, A. Y.; Vinokurov, L. M.; Lukyanov, S.; Belousov, V. V. *Bioorg. Med. Chem.* **2011**, *19*, 1079–1084.

(15) Mishina, N. M.; Tyurin-Kuzmin, P. A.; Markvicheva, K. N.; Vorotnikov, A. V; Tkachuk, V. a; Laketa, V.; Schultz, C.; Lukyanov, S.; Belousov, V. V. *Antioxid. Redox Signal.* **2011**, *14*, 1–7.

(16) Hein, B.; Willig, K. I.; Hell, S. W. *Proc. Natl. Acad. Sci. U. S. A.* **2008**, *105*, 14271–14276.

(17) Huang, B. K.; Sikes, H. D. *Redox Biol.* **2014**, *2*, 955–962.

(18) Bilan, D. S.; Pase, L.; Joosen, L.; Gorokhovatsky, A. Y.; Ermakova, Y. G.; Gadella, T. W. J.; Grabher, C.; Schultz, C.; Lukyanov, S.; Belousov, V. V. HyPer-3: *ACS Chem. Biol.* **2013**, *8*, 535–542.

(19) Rhee, S. G. *Science* **2006**, *312*, 1882–1883.

(20) Stone, J. R. *Arch. Biochem. Biophys.* **2004**, *422*, 119–124.

(21) Denu, J. M.; Tanner, K. G. *Biochemistry* **1998**, *37*, 5633–5642.

(22) Lee, S.-R. *J. Biol. Chem.* **1998**, *273*, 15366–15372.

(23) Meng, T.-C.; Fukada, T.; Tonks, N. K. *Mol. Cell* **2002**, *9*, 387–399.

(24) Ross, S. H.; Lindsay, Y.; Safrany, S. T.; Lorenzo, O.; Villa, F.; Toth, R.; Clague, M. J.; Downes, C. P.; *Cell. Signal.* **2007**, *19*, 1521–1530.

(25) Peskin, A. V.; Low, F. M.; Paton, L. N.; Maghzal, G. J.; Hampton, M. B.; Winterbourn, C. C. *J. Biol. Chem.* **2007**, *282*, 11885–11892.

(26) Winterbourn, C. C. *Nat. Chem. Biol.* **2008**, *4*, 278–286.

(27) Wood, Z. A; Schroder, E.; Robin Harris, J.; Poole, L. B. *Trends Biochem. Sci.* **2003**, *28*, 32–40.

Insert Table of Contents Graphic and Synopsis Here